

Learning to Communicate in UAV-aided Wireless Networks: Map-based Approaches

Omid Esrafilian, *Student Member, IEEE*, Rajeev Gangula, *Member, IEEE*, and David Gesbert, *Fellow, IEEE*

Abstract—We consider the scenario of a UAV-mounted flying base station providing data communication services to a number of radio nodes spread over the ground. We focus on the problem of resource-constrained UAV trajectory design with (i) optimal parameter learning and (ii) optimal data throughput as key objectives, respectively. While the problem of throughput-optimized trajectories has been addressed in prior works, the formulation of an optimized path to efficiently discover propagation parameters has not yet been addressed. When it comes to the data communication phase, the advantage of this work comes from the exploitation of a 3D city map. While the optimization of a flying path directly based on the raw map data leads to an intractable non-differentiable cost minimization problem, we introduce a novel *map compression* method allowing us to tackle the problem with standard tools. The path optimization is then combined with a node scheduling algorithm. The advantages of both the learning path optimization and the map compression method for data communication trajectory design are illustrated in an urban IoT setting.

Index Terms—UAV, drone, trajectory design, scheduling, learning, Internet of Things, 3D map.

I. INTRODUCTION

The use of drones, a.k.a unmanned aerial vehicles (UAVs) as base stations or access points in future wireless communication networks is currently gaining significant attention for its ability to yield ultra-flexible deployments, in use cases ranging from disaster recovery scenarios, coverage of flash-crowd events and data harvesting in IoT applications [1]–[4]. While research challenges dealing with the practical evaluation and realization of UAV-aided system gains abound [5], [6], the problem of determining how to best place the flying radios remains a critical and fascinating issue. When it comes to UAV placement and trajectory design problems, most existing solutions rely on simplified channel attenuation models, based on (deterministically guaranteed) line-of-sight (LoS) links [7]–[11], or predictive models for the probability of occurrence of a LoS link [12]–[14]. In the latter approach, a *global* statistical model predicts the LoS availability as a function of e.g. UAV height and distance to the user so that the UAV position can be in turn optimized to maximize a data communication metric. The advantage of the global statistical LoS model lies in its simplicity for system analysis. The drawback however lies in the lack of actual performance guarantees for an in-field deployment scenario of the placement algorithms. The key

reason for this is that, the *local* terrain topology may differ sharply from the predictions drawn from statistical features. In order to circumvent this problem, the embedding of actual 3D city map data in the UAV placement algorithms has been recently proposed [8], [9]. Map-based approaches help providing a reliable prediction of LoS availability for any pair of UAV and ground node locations, hence lead to improved performance guarantees. Yet, these go at the computational and memory costs related to processing rich additional data. So far, map-based approaches have been investigated mainly for static UAV placement, i.e. a problem where a UAV is deployed at one location allowing to efficiently communicate with not-too-distant ground nodes [8]. In many scenarios however including IoT data harvesting, there is an interest in flying along a path cycle that brings the UAV-mounted base station (BS) successively closer to each and every ground node. Up to our knowledge, this paper is the first to consider the problem of communication-oriented trajectory design while exploiting 3D map data. We consider an instance of IoT data harvesting scenario where a UAV flies over a city endowed with a number of scattered ground nodes (e.g. radio-equipped sensors). We then formulate a resource-constrained UAV trajectory design problem in order to optimize data throughput from the ground nodes in a max-min sense. In a separate additional contribution and because the data communication phase critically depends on the knowledge of radio channel parameters, we also formulate a novel optimal trajectory design problem from a *parameter learning* point of view. Specifically, our results are as follows:

- We formulate and solve a learning trajectory optimization problem in order to minimize the estimation error of the channel model parameters. The devised trajectory allows the UAV to exploit the map and efficiently learn the propagation parameters.
- Based on the learned parameters, we formulate and solve a joint trajectory and node scheduling design problem which allows to maximize the traffic communicated from each node to the UAV. An algorithm is proposed which iterates between trajectory and scheduling design updates and is shown to converge. While the algorithm exploits the possibly rich map data, it does so via a *map compression* method which renders the trajectory optimization problem differentiable and amenable to standard optimization tools, hence mitigating a known drawback of map-based approaches.
- The proposed map-compression method allows us to smooth out the map data while preserving the node

This work was supported by the ERC under the European Union Horizon 2020 research and innovation program (Agreement no. 670896).

The authors are with the Department of Communication Systems, EURECOM, Sophia-Antipolis, France (email: {esrafilian, gangula, gesbert}@eurecom.fr).

location-dependent channel behavior around that node.

- The gains brought by the exploitation of 3D map data over a pure global statistical approach are illustrated, both for channel parameters learning and the data communication problems, in the context of an urban IoT scenario.

This paper is organized as follows: Section II introduces the system model. In Section III, we formulate and solve the problem of channel parameters learning path optimization. Section IV tackles the problem of the joint trajectory and node scheduling. Numerical results are presented in Section V. Finally, Section VI concludes with some perspectives.

Notation: Matrices are represented by uppercase bold letters, vectors are represented by lowercase bold letters. The transpose of matrix \mathbf{A} is denoted by \mathbf{A}^T . The set of integers from m to n , $m < n$, is represented by $[m, n]$. $Tr[\cdot]$ represents the trace function and $E\{\cdot\}$ denotes expectation.

II. SYSTEM MODEL

A wireless communication system where a UAV-mounted flying BS serving M static ground level nodes (IoT sensors, radio terminals, etc.) in an urban area is considered. The m -th ground node, $m \in [1, M]$, is located at $\mathbf{x}_m^u = (x_m^u, y_m^u) \in \mathbb{R}^2$. The UAV/drone position is denoted by $\mathbf{x}_d = (x_d, y_d, z_d) \in \mathbb{R}^3$. We assume that the ground nodes are equipped with GPS receivers or have been placed at selected locations, hence the coordinates $\mathbf{x}_m^u, m \in [1, M]$ and \mathbf{x}_d are known at all times. The drone is assumed GPS-tracked and its position is also known.

The goal of the UAV's mission is to efficiently explore the city skies in order to learn the propagation environment parameters and exploit this information to optimize the communication services offered to the ground nodes. To keep this problem tractable, we are treating the learning and the communication phases as separated in time. The goal of the learning phase, which lasts for a predefined duration of T_l , is to design a flying trajectory where the UAV collects measurements from which the propagation channel parameters are estimated. Relying on the channel parameters estimated from the learning phase, the goal of the communication phase is to generate a UAV trajectory that maximizes the minimum amount of data collected from the ground nodes within a constrained flying time of T_c .

A. Channel Model

Classically, the channel gain between a ground node and the UAV separated by distance d meters can be modeled [15]–[17] as

$$\gamma_s = \frac{\beta_s}{d^{\alpha_s}} \times \xi_s, \quad (1)$$

where α_s is the path loss exponent, β_s is the average channel gain at the reference point $d = 1$ meter, ξ_s denotes the shadowing component, and finally $s \in \{\text{LoS}, \text{NLoS}\}$ emphasizes the strong dependence of the propagation parameters on LoS or non-line-of-sight (NLoS) scenario. The channel gain in dB can be written as

$$g_s = \beta_s - \alpha_s \varphi(d) + \eta_s, \quad (2)$$

where $g_s = 10 \log_{10} \gamma_s$, $\beta_s = 10 \log_{10} \beta_s$, $\varphi(d) = 10 \log(d)$, $\eta_s = 10 \log_{10} \xi_s$, and η_s is modeled as a Gaussian random variable with $\mathcal{N}(0, \sigma_s^2)$. It is worthy to mention that, for clarity of exposition, we do not distinguish between the NLoS scenarios according to the number of buildings which obstruct LoS line, although more precise models based on multiple propagation segments are possible [18].

B. UAV Model

In both phases, the time spans T_l and T_c are respectively discretized into N_l and N_c equally spaced time slots. The time slots are sufficiently small such that the UAV's location, velocity, and heading angles can be considered to remain constant in one slot. The drone's position evolves according to

$$\mathbf{x}_d[n] = \mathbf{x}_d[n-1] + \begin{bmatrix} \cos(\phi[n]) \cos(\psi[n]) \\ \sin(\phi[n]) \cos(\psi[n]) \\ \sin(\psi[n]) \end{bmatrix} \rho[n], \quad (3)$$

$$n \in [1, N_l] \text{ (or) } n \in [1, N_c],$$

where in the n -th time slot, $\mathbf{x}_d[n]$ denotes the position of the UAV, $0 \leq \rho[n] \leq \rho_{max}$ is the moving distance, and ρ_{max} depends on the maximum velocity. $0 \leq \phi[n] \leq 2\pi$, $-\frac{\pi}{2} \leq \psi[n] \leq \frac{\pi}{2}$ denote the heading and elevation angles, respectively.

III. OPTIMIZATION OF THE LEARNING TRAJECTORY

Using the above described models, in this section our goal is to find the UAV trajectory (over which the channel measurements are collected from the ground nodes) that results in the minimum estimation error of the channel parameters. While the problem of learning the channel parameters from a pre-determined measurement data set has been addressed in the prior literature [17], [18], the novelty of our work lies in the concept of optimizing the flight trajectory *itself* so as to accelerate the learning process. The channel measurement collection and learning process are described next.

A. Measurement Collection and Channel Learning

The measurement harvesting trajectory starts from a base position \mathbf{x}_b and ends at a terminal position¹ \mathbf{x}_t , and lasts for a duration of time T_l . We assume a time-discretized measurement process whereby the UAV flies and collects link gain measurements per ground node (every Δ meters apart). In the n -th time interval, $n \in [1, N_l]$, the collected measurements can be written as

$$\mathbf{g}_{s,n} = [g_{s,1}, \dots, g_{s,\delta_{s,n}}]^T,$$

where $g_{s,i}$ is the channel gain of the i -th measurement, $i \in [1, \delta_{s,n}]$, and $\delta_{s,n}$ is the number of measurements obtained for the propagation segment group $s \in \{\text{LoS}, \text{NLoS}\}$. Hence, the

¹The base point is typically the take-off base for the UAV while \mathbf{x}_t can be selected in different ways, including $\mathbf{x}_t = \mathbf{x}_b$ (loop) or \mathbf{x}_t coinciding with a (weighted) average of the node location is in case the communication services are to begin right after the learning phase.

total number of measurements is denoted by $D_n \triangleq \delta_{\text{LoS},n} + \delta_{\text{NLoS},n}$. For the LoS/NLoS classification of the measurements, we leverage the knowledge of a 3D city map [19]. Based on such map, we can predict LoS (un)availability on any given UAV-ground nodes link from a trivial geometry argument: For a given UAV position, the ground node is considered in LoS to the UAV if the straight line passing through the UAV's and the ground node's position lies higher than any buildings in between.

Using (2), the i -th measurement can be modeled as

$$g_{s,i} = \mathbf{a}_{s,i}^T \boldsymbol{\omega}_s + \eta_{s,i}, \quad (4)$$

where $\mathbf{a}_{s,i} = [\varphi(d^i), 1]^T$ and $\boldsymbol{\omega}_s = [\alpha_s, \beta_s]^T$ is the vector of channel parameters. Equivalently, for all measurements belonging to the n -th interval, we have

$$\mathbf{g}_{s,n} = \mathbf{A}_{s,n} \boldsymbol{\omega}_s + \boldsymbol{\eta}_{s,n}, \quad (5)$$

where $\mathbf{A}_{s,n} = [\mathbf{a}_{s,1}, \dots, \mathbf{a}_{s,\delta_{s,n}}]^T$, $\boldsymbol{\eta}_{s,n} = [\eta_{s,1}, \dots, \eta_{s,\delta_{s,n}}]^T$. Finally, we stack up the measurements gathered by the drone up to time step n as

$$\bar{\mathbf{g}}_{s,n} = \bar{\mathbf{A}}_{s,n} \boldsymbol{\omega}_s + \bar{\boldsymbol{\eta}}_{s,n}, \quad (6)$$

where $\bar{\mathbf{g}}_{s,n} = [\mathbf{g}_{s,1}^T, \dots, \mathbf{g}_{s,n}^T]^T$, $\bar{\mathbf{A}}_{s,n} = [\mathbf{A}_{s,1}^T, \dots, \mathbf{A}_{s,n}^T]^T$, $\bar{\boldsymbol{\eta}}_{s,n} = [\boldsymbol{\eta}_{s,1}^T, \dots, \boldsymbol{\eta}_{s,n}^T]^T$. Assuming that the measurements collected over a trajectory are independent, the maximum likelihood estimation [17], [19] of parameters $\boldsymbol{\omega}_s$ for each LoS/NLoS based on the measurements collected up to time step n is given by

$$\hat{\boldsymbol{\omega}}_{s,n} = (\bar{\mathbf{A}}_{s,n}^T \bar{\mathbf{A}}_{s,n})^{-1} \bar{\mathbf{A}}_{s,n}^T \bar{\mathbf{g}}_{s,n}. \quad (7)$$

By substituting (6) in (7), we obtain

$$\hat{\boldsymbol{\omega}}_{s,n} - \boldsymbol{\omega}_s = (\bar{\mathbf{A}}_{s,n}^T \bar{\mathbf{A}}_{s,n})^{-1} \bar{\mathbf{A}}_{s,n}^T \bar{\boldsymbol{\eta}}_{s,n}. \quad (8)$$

Since $\hat{\boldsymbol{\omega}}_{s,n}$ is unbiased, then the covariance of $\hat{\boldsymbol{\omega}}_{s,n}$ is given by

$$\begin{aligned} \text{Cov}\{\hat{\boldsymbol{\omega}}_{s,n}\} &= E\left\{(\hat{\boldsymbol{\omega}}_{s,n} - \boldsymbol{\omega}_s)(\hat{\boldsymbol{\omega}}_{s,n} - \boldsymbol{\omega}_s)^T\right\} \\ &= \sigma_s^2 (\bar{\mathbf{A}}_{s,n}^T \bar{\mathbf{A}}_{s,n})^{-1}. \end{aligned} \quad (9)$$

Thus, the mean square error of the estimated parameters [20] is as follows

$$\begin{aligned} E\left\{\|\hat{\boldsymbol{\omega}}_{s,n} - \boldsymbol{\omega}_s\|^2\right\} &= \text{Tr}\{\text{Cov}\{\hat{\boldsymbol{\omega}}_{s,n}\}\} \\ &= \sigma_s^2 \text{Tr}\left[(\bar{\mathbf{A}}_{s,n}^T \bar{\mathbf{A}}_{s,n})^{-1}\right]. \end{aligned} \quad (10)$$

Let

$$e_s[n] \triangleq \text{Tr}\left[(\bar{\mathbf{A}}_{s,n}^T \bar{\mathbf{A}}_{s,n})^{-1}\right],$$

and assuming that $\sigma_{\text{NLoS}}^2 = k \cdot \sigma_{\text{LoS}}^2$, $k \geq 1$ [21], the total estimation error in both propagation segments is given by

$$\sum_s E\left\{\|\hat{\boldsymbol{\omega}}_{s,n} - \boldsymbol{\omega}_s\|^2\right\} = \sigma_{\text{LoS}}^2 (e_{\text{LoS}}[N_l] + k e_{\text{NLoS}}[N_l]). \quad (11)$$

Note that a full rank $\bar{\mathbf{A}}_{s,n}$ is needed, classically. In other words, more than a critical number measurements from both LoS and NLoS categories must be collected, where again the map will prove useful

B. Learning Trajectory Design

In this section, we aim to find the optimal control policy which minimizes the learning error in equation (11). The optimization problem under start and finish locations, and total flying time, can be written as

$$\min_{\Phi, \Psi, \mathcal{R}} e_{\text{LoS}}[N_l] + k e_{\text{NLoS}}[N_l] \quad (12a)$$

$$\text{s.t. } \mathbf{x}_d[0] = \mathbf{x}_b, \mathbf{x}_d[N_l] = \mathbf{x}_t, \quad (12b)$$

$$(3), \quad (12c)$$

where N_l is the discretized trajectory vector length, clarified below. Φ, Ψ, \mathcal{R} denote the control inputs and are defined as

$$\begin{aligned} \Phi &= \{0 \leq \phi[n] \leq 2\pi, n \in [1, N_l]\}, \\ \Psi &= \left\{-\frac{\pi}{2} \leq \psi[n] \leq \frac{\pi}{2}, n \in [1, N_l]\right\}, \\ \mathcal{R} &= \{0 \leq \rho[n] \leq \rho_{max}, n \in [1, N_l]\}. \end{aligned}$$

We can rewrite $e_s[N_l]$ as follows

$$\begin{aligned} e_s[N_l] &= \text{Tr}\left[\left(\left[\begin{array}{c} \bar{\mathbf{A}}_{s,N_l-1} \\ \mathbf{A}_{s,N_l} \end{array}\right]^T \left[\begin{array}{c} \bar{\mathbf{A}}_{s,N_l-1} \\ \mathbf{A}_{s,N_l} \end{array}\right]\right)^{-1}\right] \\ &= e_s[N_l - 1] - r_s[N_l] \\ &= e_s[1] - \sum_{n=2}^{N_l} r_s[n], \end{aligned} \quad (13)$$

where we denote $r_s[n]$ as the amount of improvement in the estimate within time step n , and it is given by

$$r_s[n] = \text{Tr}\left[(\mathbf{I} + \mathbf{H}_{s,n} \mathbf{A}_{s,n}^T \mathbf{A}_{s,n})^{-1} \mathbf{H}_{s,n} \mathbf{A}_{s,n}^T \mathbf{A}_{s,n} \mathbf{H}_{s,n}\right], \quad (14)$$

where $\mathbf{H}_{s,n} = (\bar{\mathbf{A}}_{s,n-1}^T \bar{\mathbf{A}}_{s,n-1})^{-1}$ and \mathbf{I} is the identity matrix. Now we reformulate (12) as

$$\max_{\Phi, \Psi, \mathcal{R}} \sum_{n=1}^{N_l} \mathcal{I}_{\text{LoS}}[n] + k \mathcal{I}_{\text{NLoS}}[n] \quad (15a)$$

$$\text{s.t. } \mathbf{x}_d[0] = \mathbf{x}_b, \mathbf{x}_d[N_l] = \mathbf{x}_t, \quad (15b)$$

$$(3), \quad (15c)$$

where for $s \in \{\text{LoS}, \text{NLoS}\}$, and

$$\mathcal{I}_s[n] = \begin{cases} -e_s[1] & n = 1 \\ r_s[n] & n \in [2, N_l] \end{cases}.$$

The optimization over functionals makes it difficult to obtain analytic solutions for the problem in (15). Therefore, we obtain discrete approximations of the optimal trajectories by employing a dynamic programming technique [22].

1) Discrete Approximation and Dynamic Programming:

We discretize the city into a 3D grid map (hereafter termed as path graph) consisting of the UAV admissible locations. The discretization unit for creating path graph in horizontal and vertical plane is respectively denoted by a_h, a_v . An illustration of the example path graph, start, and terminal nodes is depicted in Fig. 1, for the ease of exhibition we showed the 2D case. Moreover, in order to restrain complexity, the control inputs

for any time step $n \in [1, N_l]$ are constrained to a limited alphabet:

$$\begin{aligned}\phi[n] &\in \left\{ 0, \frac{\pi}{4}, \frac{\pi}{2}, \frac{3\pi}{4}, \pi, \frac{5\pi}{4}, \frac{3\pi}{2}, \frac{7\pi}{4} \right\}, \\ \psi[n] &\in \left\{ -\frac{\pi}{2}, -\frac{\pi}{4}, 0, \frac{\pi}{4}, \frac{\pi}{2} \right\}, \\ \rho[n] &\in \left\{ 0, a_h, a_v, a_h\sqrt{2}, \sqrt{2a_h^2 + a_v^2} \right\}.\end{aligned}$$

In order not to exceed the flight time constraint T_l , N_l can be selected as ²

$$N_l = \left\lfloor \frac{T_l}{T_e} \right\rfloor,$$

where $\lfloor \cdot \rfloor$ denotes the floor function and $T_e = \frac{\sqrt{2a_h^2 + a_v^2}}{v_{max}}$, where v_{max} represents the drone maximum speed.

Forward dynamic programming is now used to solve for (15) taking into account the finite alphabet constraint [22]. Thus, we associate with our problem the performance index

$$J_i(S[i]) = \Phi(S[0]) + \sum_{n=1}^i L[n], \quad (16)$$

where $[1, i]$ is the time interval of interest and $S[i]$ denotes the state set at time step i and is defined as follows

$$S[i] = \{ \mathbf{x}_d[i], \bar{\mathbf{g}}_{LoS,i}, \bar{\mathbf{A}}_{LoS,i}, \bar{\mathbf{g}}_{NLoS,i}, \bar{\mathbf{A}}_{NLoS,i} \}, \quad n \in [1, N_l],$$

and $L[n] = \mathcal{I}_{LoS}[n] + k \mathcal{I}_{NLoS}[n]$. $\Phi(S[0])$ stands for the initial cost which is given by

$$\Phi(S[0]) = \begin{cases} 0 & \mathbf{x}_d[0] = \mathbf{x}_b \\ -\infty & \text{otherwise} \end{cases}.$$

Therefore, the optimal cost at time n on state $S[n]$ is equal to

$$J_n^*(S[n]) = \max_{\mathbf{u}[n]} \{ L[n] + J_{n-1}^*(S[n-1]) \}, \quad n \in [1, N_l], \quad (17)$$

$$J_0^*(S[0]) = \Phi(S[0]), \quad (18)$$

where $\mathbf{u}[n] = [\phi[n], \psi[n], \rho[n]]^T$, $n \in [1, N_l]$ is the input control vector. Thus, the optimal control input $\mathbf{u}^*[n]$ at time n is the one that achieves the maximum in (17). Finally, the optimal policy (trajectory) can be found by solving (17) for all $n \in [1, N_l]$ under final state constraint $\mathbf{x}_d[N_l] = \mathbf{x}_t$.

IV. COMMUNICATION TRAJECTORY OPTIMIZATION

Based on the acquired knowledge of the channel parameters obtained from the learning phase, we are now concerned with the design of a *communication trajectory* which maximizes a throughput performance metric for an uplink IoT scenario. For ease of exposition, the communication phase is designed based on the perfect channel model parameter estimates, while the impact of imperfect estimation is addressed in Section V. For the trajectory optimization, we use the same framework as [11]

²Note that this is a conservative choice. In practice, N_l could be slightly higher given the UAV may use some of the short edges.

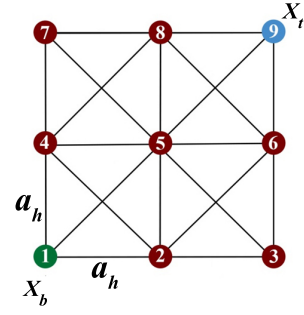


Figure 1. Path graph depicted in 2D. Here the example start vertex is 1 and target destination is vertex 9.

by employing the block-coordinate descent [23] and sequential convex programming [24] techniques while the key differences are that we optimize the drone's altitude, and also exploit the 3D city map by introducing a statistical map compression approach that enables us to take into account the LoS and NLoS predictions.

A. Communication System Model

We assume that the M ground nodes are served by the drone in a time-division multiple access manner. In order to keep notations simple, we assume the scheduling granularity is the same as the time sampling rate³, such that at every time step only one node gets the chance of sending some data to the drone which yields the following constraints

$$\sum_{m=1}^M q_m[n] \leq 1, \quad n \in [1, N_c], \quad (19)$$

$$q_m[n] \in \{0, 1\}, \quad n \in [1, N_c], \quad m \in [1, M], \quad (20)$$

where $q_m[n]$ is the scheduling variable, $q_m[n]=1$ indicates that the ground node m is scheduled at time step n . The achievable ergodic rate for the m -th ground node when scheduled in the n -th time slot is

$$C_m[n] = E \left\{ \log_2 \left(1 + \frac{p\gamma_m[n]}{\sigma^2} \right) \right\}, \quad (21)$$

where $\gamma_m[n]$ is the channel gain between the m -th node and the UAV at time step n , p denotes the up-link transmission power, and the additive white Gaussian noise power at the receiver is denoted by σ^2 . The average achievable throughput of the m -th ground node towards the UAV over the course of the communication phase is given by

$$C_m = \frac{1}{N_c} \sum_{n=1}^{N_c} q_m[n] C_m[n], \quad m \in [1, M]. \quad (22)$$

B. Joint Scheduling and Path Optimization

The problem of maximizing the minimum average rate among all ground nodes by jointly optimizing node scheduling and UAV trajectory can be formulated as

³This is by no means a restriction and more general notation could be accommodated with similar principles.

$$\max_{\mathcal{X}_d, z_d, Q, \mu} \mu \quad (23a)$$

$$\text{s.t. } C_m \geq \mu, m \in [1, M], \quad (23b)$$

$$\|\mathbf{x}_d[n] - \mathbf{x}_d[n-1]\| \leq \rho_{max}, n \in [2, N_c], \quad (23c)$$

$$\mathbf{x}_d[1] = \mathbf{x}_d[N_c], \quad (23d)$$

$$z_d \geq h_{min}, \quad (23e)$$

$$(19), (20), \quad (23f)$$

where $Q = \{q_m[n], \forall n, \forall m\}$, and $\mathcal{X}_d = \{(x_d[n], y_d[n]), \forall n\}$ is the UAV discretized path vector of length N_c in 2D. We assume that the drone flies at a fixed altitude z_d to be optimized as well. The maximum speed constraint on the UAV is reflected in (23c), where $\rho_{max} = \frac{v_{max} T_c}{N_c}$. (23d) implies a possible loop trajectory constraint, and the constraint in (23e) forces the drone to fly above all the city's buildings where h_{min} is the height of the tallest building in the city.

Problem (23) is challenging to solve due to the following issues: Firstly, ground node scheduling variables are binary and include integer constraints. Secondly, (23b) is a non-convex constraint with respect to the drone trajectory variables. Moreover by assuming the 3D city map, node locations, and UAV location at time n are known, then in theory the LoS or NLoS status of the link can be finely predicted and, hence, the link gain $\gamma_m[n]$ can be computed from (1) up to the random shadowing. Unfortunately, such a direct exploitation of the rich raw map data leads to a highly non-differentiable problem in (23).

C. LoS Probability Model Using Map Compression

To tackle the problem of non-differentiability arising from the exploitation of the 3D map, we propose a new approach coined (*statistical*) *map compression* which aims at smoothing out the map data while preserving essential *node-location dependent* channel behavior. The map compression approach relies on converting map data to build a reliable node location dependent LoS probability model. For the link between the drone located at altitude z_d and the m -th ground node in the n -th time slot, the LoS probability is now given by

$$p_m[n] = \frac{1}{1 + \exp(-a_m \theta_m[n] + b_m)}, \quad (24)$$

where $\theta_m[n] = \arctan(z_d/r_m[n])$ denotes the elevation angle and $r_m[n]$ is the ground projected distance between the drone and the m -th node located at \mathbf{x}_m^u in time slot n , and $\{a_m, b_m\}$ are the model coefficients.

The LoS probability model coefficients $\{a_m, b_m\}$ are learned (i.e. by utilizing logistic regression method [20]) by using a training data set formed by a set of tentative UAV locations around the m -th ground node along with the true LoS/NLoS label obtained from the 3D map. Interestingly, the model in (24) can be seen as a localized extension of the classical (global) UAV probability model used in [12]–[14]. The key difference lies in the fact that, a *local* LoS probability model will give performance guarantees which a global model cannot give.

Using (24), the average channel gain of the link between the drone and the m -th ground node in the n -th time slot can easily be shown to be

$$E\{\gamma_m[n]\} = \left(\frac{d_m^{(A-1)\alpha_{LoS}} - B}{1 + \exp(-a_m \theta_m + b_m)} + B \right) \frac{\beta_{LoS}}{d_m^{\alpha_{NLoS}}}, \quad (25)$$

where $B = \frac{\beta_{NLoS}}{\beta_{LoS}}$, $A = \frac{\alpha_{NLoS}}{\alpha_{LoS}} \geq 1$, and $d_m[n] = \sqrt{z_d^2 + r_m^2[n]}$ is the distance between the m -th ground node and the drone. The details of the proof are given in Appendix A. Note that, the average random shadowing is assumed absorbed into β_s , $s \in \{\text{LoS}, \text{NLoS}\}$ to ease notation.

We can use the above to upper bound the achievable throughput of the drone-ground node link at time slot n as follows:

$$C_m[n] \leq C_m^{\text{up}}[n] = \log_2 \left(1 + \frac{p \cdot E\{\gamma_m[n]\}}{\sigma^2} \right), \quad (26)$$

where the upper-bounding argument originates from the Jensen's inequality. The average throughput upper-bound then can be written as

$$C_m^{\text{up}} = \frac{1}{N_c} \sum_{n=1}^{N_c} q_m[n] C_m^{\text{up}}[n], m \in [1, M]. \quad (27)$$

Finally, we can simplify the original problem (23) into the follow *map-compressed* problem:

$$\max_{\mathcal{X}_d, z_d, Q, \mu} \mu \quad (28a)$$

$$\text{s.t. } C_m^{\text{up}} \geq \mu, \forall m, \quad (28b)$$

$$0 \leq q_m[n] \leq 1, \forall m, n, \quad (28c)$$

$$(23c), (23d), (23e), (19), \quad (28d)$$

where map compression allowed us to circumvent the non-differentiability aspect of the original problem (23) because of substituting (25) in (26) leads to a differentiable function C_m^{up} with respect to the m -th ground node location and the drone position. Moreover for further simplification, we relaxed the binary scheduling variable into continuous variables which is mentioned in (28c). However, (28) is still difficult to solve since it is a joint scheduling and path planning problem and is not convex. To make this problem more tractable, we split it up into two optimization sub-problems and then classically iterate between them to converge to the final solution. Note that, the iteration index of the proposed algorithm is denoted by “ j ”.

D. Scheduling

For a given UAV trajectory \mathcal{X}_d and altitude z_d , the ground node scheduling can be optimized along the following lines:

$$\max_{Q, \mu} \mu \quad (29a)$$

$$\text{s.t. } \frac{1}{N_c} \sum_{n=1}^{N_c} q_m[n] C_m^{\text{up}}[n] \geq \mu, \forall m, \quad (29b)$$

$$\sum_{m=1}^M q_m[n] \leq 1, \forall n, \quad (29c)$$

$$0 \leq q_m[n] \leq 1, \forall m, n. \quad (29d)$$

This problem is a standard one in the literature [25]–[27] that has the form of a Linear Programming (LP) problem.

E. Communication Path Optimization

For a given scheduling decision Q , we now aim to find the optimal trajectory. While the optimal trajectory in (28) involves a challenging 3D search, we choose to limit our search to planar trajectories, which allows us to decouple the 2D trajectory design from the altitude search.

1) *Optimal Horizontal UAV Trajectory*: The optimal UAV trajectory by assuming a fixed flying altitude z_d can be obtained by solving

$$\max_{\mathcal{X}_d, \mu} \mu \quad (30a)$$

$$\text{s.t. } C_m^{\text{up}} \geq \mu, \forall m, \quad (30b)$$

$$(23c), (23d). \quad (30c)$$

The optimization problem (30) is not convex, since the constraint (30b) is neither convex nor concave. In general, there is no efficient method to obtain the optimal solution. Therefore, we adopt sequential convex optimization technique for the trajectory optimization. To this end, the following results are helpful.

Lemma 1. *The function $h(x, y) \triangleq \log(1 + f(x)g(y))$ is convex if $\hat{h}(x, y) = \log(f(x)g(y))$ is convex and $f(x) > 0, g(y) > 0$.*

Proof. See Appendix B. \square

Proposition 1. *For any constant $\alpha, k > 0$, the function $\log\left(1 + \left[\left(\frac{1}{1+x}\right)\left(\frac{1}{y}\right) + k\right]\frac{1}{d^\alpha}\right)$ is convex.*

Proof. See Appendix C. \square

By defining the auxiliary variables $f_m[n], g_m[n], l_m[n]$, and $\theta_m[n]$, we can rewrite (30) as follows

$$\max_{\mathbb{V}, \mathcal{X}_d, \mu} \mu \quad (31a)$$

$$\text{s.t. } \frac{1}{N_c} \sum_{n=1}^{N_c} c_m(f_m[n], g_m[n], l_m[n]) \geq \mu, \forall m, \quad (31b)$$

$$g_m[n] = \left((z_d^2 + l_m[n])^{\frac{(A-1)\alpha_{\text{LoS}}}{2}} - B \right)^{-1}, \forall m, n, \quad (31c)$$

$$f_m[n] = \exp(-a_m \theta_m[n] + b_m), \forall m, n, \quad (31d)$$

$$l_m[n] = r_m^2[n], \forall m, n, \quad (31e)$$

$$\theta_m[n] = \tan^{-1}\left(\frac{z_d}{\sqrt{l_m[n]}}\right), \forall m, n, \quad (31f)$$

$$f_m[n], g_m[n], l_m[n], \theta_m[n] \geq 0, \forall m, n, \quad (31g)$$

$$(23c), (23d), \quad (31h)$$

where $\mathbb{V} = \{f_m[n], g_m[n], l_m[n], \theta_m[n] | \forall m, n\}$ consists of all the auxiliary variables and

$$c_m(f_m[n], g_m[n], l_m[n]) \triangleq$$

$$\log_2 \left(1 + \left(\frac{\frac{1}{g_m[n]}}{(1 + f_m[n])} + B \right) \frac{p\beta_{\text{LoS}}}{\sigma^2 (z_d^2 + l_m[n])^{\frac{\alpha_{\text{NLoS}}}{2}}} \right). \quad (32)$$

Using Proposition 1, it can be easily seen that (32) is a convex function of variables $f_m[n], g_m[n]$, and $l_m[n]$. In constraint (31c), $g_m[n]$ can be convex or concave function depends on the value of B where according to our simulations, it is always convex since in an urban dense city we consider $h_{\text{min}} > B$. Moreover, all constraints (31d) to (31f) comprise convex functions. In order to solve the problem (31), we utilize the sequential convex programming technique which solves instead the local linear approximation of the original problem. To form the local linear approximation, we use the given variables \mathcal{X}_d^j, z_d^j in the j -th iteration of the algorithm to convert the above problem to a standard convex form. For the ease of exposition, we use $c_m[n]$ instead of $c_m(f_m[n], g_m[n], l_m[n])$. First, let's start with constraint (31b), since any convex function can be lower-bounded by it's first order Taylor expansion, then we can write

$$\frac{1}{N_c} \sum_{n=1}^{N_c} q_m[n] c_m[n] \geq \frac{1}{N_c} \sum_{n=1}^{N_c} q_m[n] \tilde{c}_m[n] \geq \mu_{hp},$$

where $\tilde{c}_m[n]$ is an affine function and equals to the local first order Taylor expansion of $c_m[n]$ and μ_{hp} is a lower bound of μ . Similarly, We can convert all constraints (31c) to (31f) into the standard convex form by replacing them with their first order Taylor expansion. Finally, we can approximate problem (31) as follows

$$\max_{\mathbb{V}, \mathcal{X}_d, \mu_{hp}} \mu_{hp} \quad (33a)$$

$$\text{s.t. } \frac{1}{N_c} \sum_{n=1}^{N_c} q_m[n] \tilde{c}_m[n] \geq \mu_{hp}, \forall m, \quad (33b)$$

$$f_m[n] \geq \tilde{f}_m[n], \forall m, n, \quad (33c)$$

$$g_m[n] \geq \tilde{g}_m[n], \forall m, n, \quad (33d)$$

$$l_m[n] \geq \tilde{l}_m[n], \forall m, n, \quad (33e)$$

$$\theta_m[n] \geq \tilde{\theta}_m[n], \forall m, n, \quad (33f)$$

$$(31g), (23c), (23d), \quad (33g)$$

where the superscript “ \sim ” denotes the local first order Taylor expansion. Now, we have a standard convex problem which can be solved by any standard convex optimization tools like CVX [28]. We denote the generated trajectory by solving (33) as \mathcal{X}_d^{j+1} .

2) *Optimal UAV Altitude*: Now we proceed to optimize the UAV altitude for a given horizontal UAV trajectory \mathcal{X}_d . The UAV altitude optimization problem is given by

$$\max_{z_d, \mu} \mu \quad (34a)$$

$$\text{s.t. } C_m^{\text{up}} \geq \mu, \forall m, \quad (34b)$$

$$z_d \geq h_{\text{min}}. \quad (34c)$$

This problem is also not convex. By introducing auxiliary variables $h, e_m[n]$, and $g_m[n]$, the optimization problem (34) can be reformulated as

$$\max_{\mathbb{W}, z_d, \mu} \mu \quad (35a)$$

$$\text{s.t. } \frac{1}{N_c} \sum_{n=1}^{N_c} c_m(e_m[n], g_m[n], h) \geq \mu, \quad \forall m, \quad (35b)$$

$$e_m[n] = \exp\left(-a_m \tan^{-1}\left(\frac{z_d}{r_m[n]}\right) + b_m\right), \quad \forall m, n, \quad (35c)$$

$$g_m[n] = \left(\left(h + r_m^2[n]\right)^{\frac{(A-1)\alpha_{\text{LoS}}}{2}} - B\right)^{-1}, \quad \forall m, n, \quad (35d)$$

$$h = z_d^2, \quad (35e)$$

$$z_d \geq h_{\min}, \quad (35f)$$

where $c_m(e_m[n], g_m[n], h)$ is a convex function and is defined as follows

$$c_m(e_m[n], g_m[n], h) = \log_2\left(1 + \left(\frac{\frac{1}{g_m[n]}}{(1 + e_m[n])} + B\right) \frac{p\beta_{\text{LoS}}}{\sigma^2 (h + r_m^2[n])^{\frac{\alpha_{\text{NLoS}}}{2}}}\right). \quad (36)$$

The convexity argument of $c_m(e_m[n], g_m[n], h)$ is proved by Proposition 1. $\mathbb{W} = \{e_m[n], g_m[n], h \mid \forall m, n\}$ comprises all the auxiliary variables. Also, constraints (35c) to (35e) consist of convex functions. Similar to section IV-E1, we solve this problem by converting it to a standard convex form using the sequential convex programming with given local point z_d^j in the j -th iteration and the generated horizontal trajectory \mathcal{X}_d^{j+1} in the last section. Equivalently, the UAV altitude can be optimized as follows

$$\max_{\mathbb{W}, z_d, \mu_{\text{alt}}} \mu_{\text{alt}} \quad (37a)$$

$$\text{s.t. } \frac{1}{N_c} \sum_{n=1}^{N_c} q_m[n] \tilde{c}_m[n] \geq \mu_{\text{alt}}, \quad \forall m, \quad (37b)$$

$$e_m[n] \geq \tilde{e}_m[n], \quad \forall m, n, \quad (37c)$$

$$g_m[n] \geq \tilde{g}_m[n], \quad \forall m, n, \quad (37d)$$

$$h \geq \tilde{h}, \quad (37e)$$

$$e_m[n], g_m[n], h > 0, \quad (37f)$$

$$z_d \geq h_{\min}, \quad (37g)$$

where the superscript “ \sim ” denotes the local first order Taylor expansion, $\tilde{c}_m[n]$ stands for the first order Taylor expansion of $c_m(e_m[n], g_m[n], h)$, and μ_{alt} is a lower bound of μ . We denote the drone altitude which is obtained by solving (37) as z_d^{j+1} to be used in the next iteration.

3) *Iterative Algorithm*: According to the preceding analysis, now we propose an iterative algorithm to solve the original optimization problem (23) by applying the block-coordinate descent method [23]. As mentioned earlier, we split up our problem into three phases (or blocks) of ground node scheduling, drone horizontal trajectory design, and flying altitude optimization over variables $\{Q, \mathcal{X}_d, z_d\}$. In each iteration, we update just one variables set at a time, rather than updating all the variables together, by fixing the other two variables sets. Then, the output of each phase is used as an input for the next step. The rigorous description of this algorithm is summarized in Algorithm 1.

Algorithm 1 Iterative algorithm for solving optimization problem (23).

- 1) Initialize all variables $\{Q^j, \mathcal{X}_d^j, z_d^j\}, j = 1$.
- 2) Find the optimal solution of the scheduling problem (29) for given $\{\mathcal{X}_d^j, z_d^j\}$. Denote the optimal solution as Q^{j+1} .
- 3) Generate the optimal communication trajectory in horizontal plane (\mathcal{X}_d^{j+1}) by solving (33) with given variables $\{Q^{j+1}, \mathcal{X}_d^j, z_d^j\}$.
- 4) Solving optimization problem (37) given variables $\{Q^{j+1}, \mathcal{X}_d^{j+1}, z_d^j\}$ and denote the solution as z_d^{j+1} .
- 5) Update $j := j + 1$.
- 6) Go to step 2 and repeat until the convergence (i.e. until observing a small increase in objective value).

4) *Proof of Convergence* : In this section we prove the convergence of Algorithm 1 in a similar manner of [11]. To this end, in the j -th iteration we denote the $\mu(Q^j, \mathcal{X}_d^j, z_d^j)$, $\mu_{\text{hp}}(Q^j, \mathcal{X}_d^j, z_d^j)$, $\mu_{\text{alt}}(Q^j, \mathcal{X}_d^j, z_d^j)$ as the optimal objective values of problems (29), (33), and (37), respectively. From step (2) of Algorithm 1 for the given solution Q^{j+1} , we have

$$\mu(Q^j, \mathcal{X}_d^j, z_d^j) \leq \mu(Q^{j+1}, \mathcal{X}_d^j, z_d^j),$$

since the optimal solution of problem (29) is obtained. Moreover, we can write

$$\begin{aligned} \mu(Q^{j+1}, \mathcal{X}_d^j, z_d^j) &\stackrel{(a)}{=} \mu_{\text{hp}}(Q^{j+1}, \mathcal{X}_d^j, z_d^j) \\ &\stackrel{(b)}{\leq} \mu_{\text{hp}}(Q^{j+1}, \mathcal{X}_d^{j+1}, z_d^j) \\ &\stackrel{(c)}{\leq} \mu(Q^{j+1}, \mathcal{X}_d^{j+1}, z_d^j). \end{aligned}$$

Step (a) holds due to $\mu_{\text{hp}}(Q^{j+1}, \mathcal{X}_d^j, z_d^j)$ being a tight local first order Taylor approximation of problem (28) at the local points. step (b) is true, since we can find the optimal solution of problem (33) with the given variables $\{Q^{j+1}, \mathcal{X}_d^j, z_d^j\}$, and (c) holds because $\mu_{\text{hp}}(Q^{j+1}, \mathcal{X}_d^{j+1}, z_d^j)$ is the lower bound of the objective value $\mu(Q^{j+1}, \mathcal{X}_d^{j+1}, z_d^j)$. Then, by proceeding to step (4) of Algorithm 1 and given variables $\{Q^{j+1}, \mathcal{X}_d^{j+1}, z_d^j\}$, we obtain

$$\begin{aligned} \mu(Q^{j+1}, \mathcal{X}_d^{j+1}, z_d^j) &\stackrel{(d)}{=} \mu_{\text{alt}}(Q^{j+1}, \mathcal{X}_d^{j+1}, z_d^j) \\ &\stackrel{(e)}{\leq} \mu_{\text{alt}}(Q^{j+1}, \mathcal{X}_d^{j+1}, z_d^{j+1}) \\ &\stackrel{(f)}{\leq} \mu(Q^{j+1}, \mathcal{X}_d^{j+1}, z_d^{j+1}). \end{aligned}$$

Step (d) is true since the local first order Taylor approximation in (37) is tight for the given local variables $\{Q^{j+1}, \mathcal{X}_d^{j+1}, z_d^j\}$. (e) holds since, the optimization problem (37) can be optimally solved, and (f) is true due to $\mu_{\text{alt}}(Q^{j+1}, \mathcal{X}_d^{j+1}, z_d^{j+1})$ is a lower bound of the objective value $\mu(Q^{j+1}, \mathcal{X}_d^{j+1}, z_d^{j+1})$.

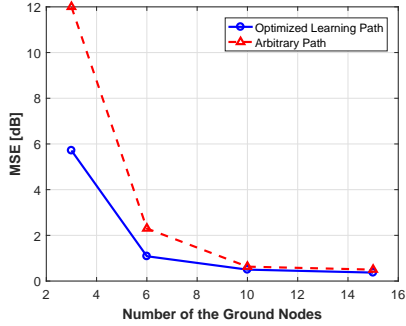


Figure 2. Comparison of the MSE for different learning paths.

Finally, we have

$$\mu(Q^j, \mathcal{X}_d^j, z_d^j) \leq \mu(Q^{j+1}, \mathcal{X}_d^{j+1}, z_d^{j+1}).$$

Which indicates that the objective value of Algorithm 1 after each iteration is non-decreasing and since it is upper bounded by a finite value, so the convergence of Algorithm 1 is guaranteed.

F. Trajectory Initializing

In this section, we propose a simple strategy to initialize the drone trajectory to be optimized later on by the introduced Algorithm 1. The initial path is in form of a circle which is centered at $\mathbf{c}_{\text{path}} = (x_{\text{path}}, y_{\text{path}})$ and the radius r_{path} which is given by

$$r_{\text{path}} = \frac{L_{\text{max}}}{2\pi},$$

where $L_{\text{max}} = T_c \cdot v_{\text{max}}$. To determine the \mathbf{c}_{path} , we use the notion of the (weighted) center of gravity [8]. Furthermore, we initialize the flying altitude as the lowest height such that the drone can on an average establish LoS links to most of the ground nodes while it is flying along the initial circular path (i.e. the average LoS probability for each ground node with respect to the drone along the circular path is greater than a threshold value τ).

V. NUMERICAL RESULTS

We consider a dense urban Manhattan-like area of size 600×600 square meters, consisting of a regular street grid and buildings with uniform random height in the range of 5 to 40 meters. True propagation parameters for the ground nodes are chosen as $\alpha_{\text{LoS}} = 2.2$, $\alpha_{\text{NLoS}} = 3.3$, $\beta_{\text{LoS}} = -26$ dB, $\beta_{\text{NLoS}} = -41$ dB. The variances of the observation noise are $\sigma_{\text{LoS}}^2 = 2$ and $\sigma_{\text{NLoS}}^2 = 5$. The transmission power for ground nodes is chosen as $p = 30$ dBm, and the noise power is -70 dBm. The UAV has a maximum speed of $v_{\text{max}} = 10$ m/s.

In Fig. 2 we present the mean square error (MSE) of the learned channel parameters ($\alpha_s, \beta_s; s = \{\text{LoS}, \text{NLoS}\}$) resulting from the measurements gathered by the drone while flying along the optimized learning path as a function of number of ground nodes. To create the 3D path graph, we chose $a_h = 100$ m and $a_v = 20$ m as defined in section III-B1. Also, we compare the performance of the learning results from the Monte-Carlo simulations over random paths

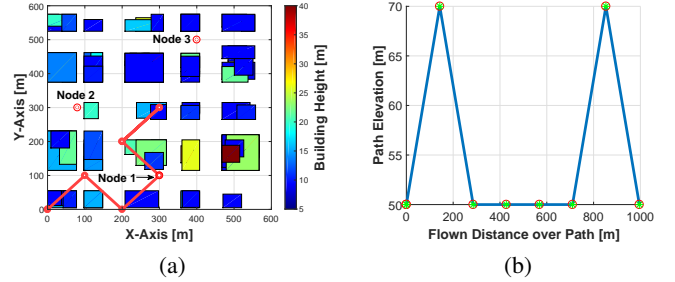


Figure 3. (a) Top view of the optimal learning trajectory using proposed algorithm. (b) The path elevation along the trajectory.

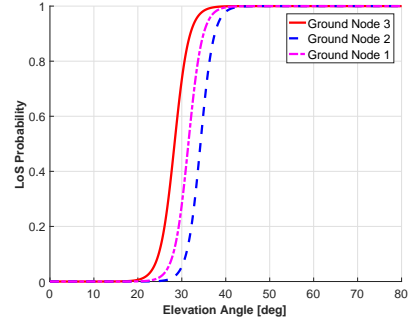


Figure 4. Local LoS probability learned from the 3D map for the ground nodes.

with the same lengths as the optimized learning trajectory which is illustrated by the dashed-line in Fig. 2. It is clear that, the channel can be learned more precisely by taking the optimized learning trajectory. Also, the learning error is reduced when the number of ground nodes increases, since the chance of obtaining measurement from both channels increases. Fig. 3 shows an example of the generated learning path for 3 random ground nodes. In this scenario, the UAV flies from the base point $\mathbf{x}_b(0, 0, 50)$ towards the terminal location $\mathbf{x}_t = (300, 300, 50)$ under the flight time constraint $T_l = 100$ sec. It is interesting to note that, the algorithm tries to improve the learning performance of both LoS and NLoS channels from experiencing a wide array of altitudes. For the ease of exhibition, we plotted the generated path in two different figures. In Fig. 3-a the top view of the generated path is shown while in Fig. 3-b the path elevation as a function of the flown distance is depicted.

Now we evaluate the performance of the ground node scheduling and communication path planning algorithm in which there are $M = 3$ nodes to be served by the drone. To learn the probability model coefficients in (24), we employed the logistic regression method on the training data set obtained by randomly sampling around each ground node along with the true LoS status obtained from the 3D city map. The local LoS probability which is learned from the 3D map for each ground node versus the elevation angle is depicted in Fig. 4.

In Fig. 5, we show the generated trajectory over the city buildings for different path lengths L_{max} . It is clear that by increasing the L_{max} , the UAV exploits the flight time to improve the ground node link quality by enlarging the trajectory and moving towards the ground nodes. It is crucial

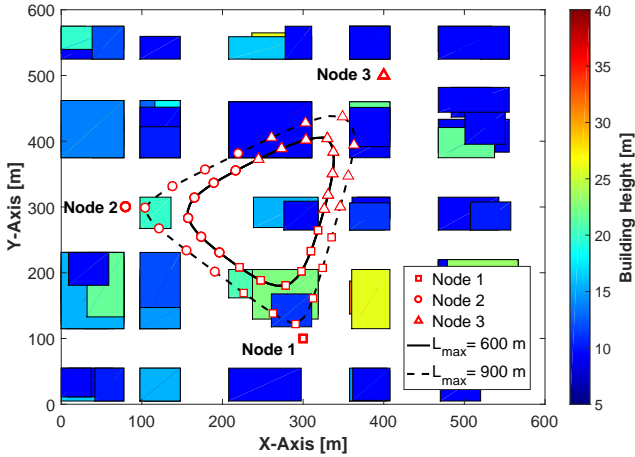


Figure 5. Optimal drone trajectory design and ground node scheduling for different path lengths. As the length increases, the UAV gets closer to individual ground nodes

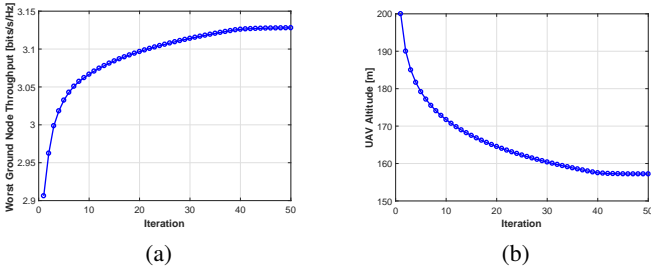


Figure 6. (a) Throughput performance versus iteration and (b) drone altitude evolution versus iteration.

to note that, the generated trajectory is closer to the ground nodes which has the less LoS probability (i.e the ground nodes who are close to buildings or surrounded by tall skyscrapers). In Fig. 5, the drone tries to get closer to the ground nodes 1 and 2 since they are close to the buildings which mostly block the LoS link to the drone. Moreover, we illustrated the result of the ground node scheduling during the trajectory with different markers which are assigned to each node. Namely triangles, squares, and circles respectively pertain to ground nodes 1 to 3. For example, square markers on the drone's trajectory indicate that the drone is serving the ground node 1.

Then, we outline the convergence behavior of Algorithm 1 by assuming $M = 3$ and $L_{max} = 900$ m. The drone altitude and worst ground nodes throughput versus iteration are shown in Fig.6. As we expected, the worst ground node throughput in each iteration improves and finally converges to a finite value.

In Fig. 7, we depicted a comparison between the map-based algorithm and the probabilistic approach versus increasing the length of the trajectory by considering the $M = 6$ ground nodes. In the probabilistic approach, we consider the same algorithm with the difference that for a link between the drone located at altitude z_d and the m -th ground node, the LoS probability at time step n is given by

$$p_m[n] = \frac{1}{1 + \exp(-a\theta_m[n] + b)},$$

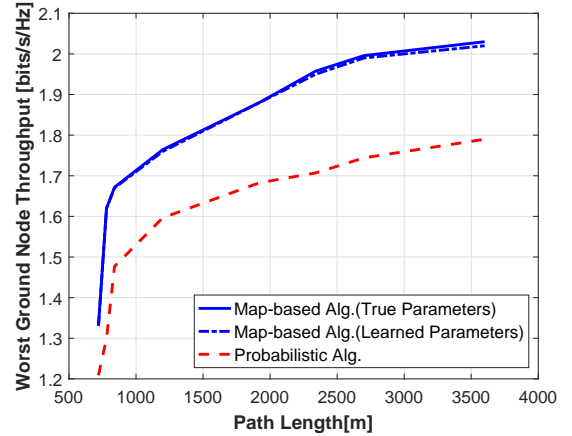


Figure 7. Performance of the map-based algorithm for learned and true channel parameters in comparison with the probabilistic approach for 6 ground nodes versus increasing the length of the drone trajectory.

In other words, we use a global LoS probability which is same for all ground nodes.

Also, we investigated the impact of the imperfect estimation of the channel parameters on the performance of the map-based algorithm. The result of the algorithm using the learned channel parameters is illustrated by the dashed-dotted line while the solid line pertains to the algorithm's output by utilizing the true channel parameters. As it can be seen, the channel estimation uncertainty stemming from the learning part has a minor effect on the performance of the map-based algorithm and in general the map-based algorithm outperforms the probabilistic approach.

VI. CONCLUSION

We considered an IoT scenario of a UAV-mounted flying base station providing data communication services to a number of radio nodes scattered over the ground. We investigated the problem of trajectory design respectively for optimal propagation parameters learning and network throughput maximization as key objectives. While the problem of throughput-optimized trajectories has been addressed in prior works, the formulation of an optimized path to efficiently learn the propagation parameters has been overlooked so far. The advantage of this work is to utilize the 3D city map which leads to an intractable non-differentiable optimization problem. To tackle this problem, we introduced a novel map compression method which renders the problem amenable to standard optimization tools.

APPENDIX

A. Proof of the average channel gain

The average channel gain of the link between the drone and the m -th ground node in the n -th time slot is given by

$$E\{\gamma_m[n]\} = \sum_s p_{s,m}[n] \gamma_{s,m}[n], \quad (38)$$

where $p_{s,m}[n], \gamma_{s,m}[n]$ are respectively the probability of occurrence and the channel gain of a certain propagation group $s \in \{\text{LoS}, \text{NLoS}\}$ for the link between the drone and the m -th ground node. According to (24), $p_{s,m}[n]$ is as follows

$$p_{\text{LoS},m}[n] = p_m[n], \quad (39)$$

$$p_{\text{NLoS},m}[n] = 1 - p_{\text{LoS},m}[n] = 1 - p_m[n]. \quad (40)$$

Then we rewrite (38) as

$$\begin{aligned} E\{\gamma_m[n]\} &\stackrel{(a)}{=} p_m[n] \frac{\beta_{\text{LoS}}}{d_m^{\alpha_{\text{LoS}}}[n]} + (1 - p_m[n]) \frac{\beta_{\text{NLoS}}}{d_m^{\alpha_{\text{NLoS}}}[n]} \\ &\stackrel{(b)}{=} \left(\frac{d_m^{(A-1)\alpha_{\text{LoS}}} - B}{1 + \exp(-a_m\theta_m + b_m)} + B \right) \frac{\beta_{\text{LoS}}}{d_m^{\alpha_{\text{LoS}}}}, \end{aligned} \quad (41)$$

where step (a) holds by substituting (39) and (40) into (38), then step (b) is obtained by some simplifications where $B = \frac{\beta_{\text{NLoS}}}{\beta_{\text{LoS}}}$, $A = \frac{\alpha_{\text{NLoS}}}{\alpha_{\text{LoS}}} \geq 1$, and $d_m[n] = \sqrt{z_d^2 + r_m^2[n]}$ is the distance between the m -th ground node and the drone.

B. Proof of Lemma 1

From the convexity assumption of $\hat{h}(x, y)$, we can write

$$\nabla^2 \hat{h} = \begin{bmatrix} \frac{f_{xx}f - f_x^2}{f^2} & 0 \\ 0 & \frac{g_{yy}g - g_y^2}{g^2} \end{bmatrix} \geq 0, \quad (42)$$

where $\nabla^2 \hat{h}$ denotes the hessian matrix and f, g stands for $f(x), g(y)$, respectively. By assuming $f, g > 0$ we can obtain

$$\frac{f_{xx}f - f_x^2}{f^2} \geq 0 \Rightarrow f_{xx} \geq \frac{f_x^2}{f} \geq 0, \quad (43)$$

$$\frac{g_{yy}g - g_y^2}{g^2} \geq 0 \Rightarrow g_{yy} \geq \frac{g_y^2}{g} \geq 0. \quad (44)$$

Also, it can be deduced that

$$f_{xx}g \geq 0, \quad g_{yy}f \geq 0, \quad (45)$$

where $f_x = \frac{\partial f}{\partial x}$, $g_y = \frac{\partial g}{\partial y}$, $f_{xx} = \frac{\partial^2 f}{\partial x^2}$, and $g_{yy} = \frac{\partial^2 g}{\partial y^2}$ are the first and second derivative of $f(x), g(y)$, respectively. Then the hessian of h is

$$\nabla^2 h = \begin{bmatrix} \frac{g^2(f_{xx}f - f_x^2) + f_{xx}g}{(1+fg)^2} & \frac{f_x g_y}{(1+fg)^2} \\ \frac{f_x g_y}{(1+fg)^2} & \frac{f^2(g_{yy}g - g_y^2) + g_{yy}f}{(1+fg)^2} \end{bmatrix}.$$

It follows from [29], that a matrix $\mathbf{W} \in \mathbb{R}^{2 \times 2}$ is positive semi-definite (PSD) if $\det(\mathbf{W}) \geq 0$ and $Tr(\mathbf{W}) \geq 0$. So, we first prove that $\det(\nabla^2 h) \geq 0$. For this, we rewrite $\nabla^2 h = \mathbf{M}_1 + \mathbf{M}_2$, where $\mathbf{M}_1, \mathbf{M}_2$ are defined as follows

$$\mathbf{M}_1 = \begin{bmatrix} \frac{g^2(f_{xx}f - f_x^2)}{(1+fg)^2} & 0 \\ 0 & \frac{f^2(g_{yy}g - g_y^2)}{(1+fg)^2} \end{bmatrix},$$

$$\mathbf{M}_2 = \begin{bmatrix} \frac{f_x g_y}{(1+fg)^2} & \frac{f_x g_y}{(1+fg)^2} \\ \frac{f_x g_y}{(1+fg)^2} & \frac{g_{yy}f}{(1+fg)^2} \end{bmatrix}.$$

From [30], for any 2×2 matrix we have $\det(\mathbf{A} + \mathbf{B}) = \det(\mathbf{A}) + \det(\mathbf{B}) + Tr(\mathbf{A}^\dagger \mathbf{B})$, where \mathbf{A}^\dagger is the adjugate of \mathbf{A} . thus, we can write

$$\det(\nabla^2 h) = \det(\mathbf{M}_1) + \det(\mathbf{M}_2) + Tr(\mathbf{M}_1^\dagger \mathbf{M}_2).$$

From (42), it can easily be shown that $\det(\mathbf{M}_1) \geq 0$. Also, we can write that $\det(\mathbf{M}_2) = (1 + fg)^{-2} [(f_{xx}f) \cdot (g_{yy}g) - f_x^2 g_y^2]$. According to (43) and (44), we have

$$f_{xx}f \geq f_x^2, \quad g_{yy}g \geq g_y^2, \quad (46)$$

which yields $\det(\mathbf{M}_2) \geq 0$. Finally, $Tr(\mathbf{M}_1^\dagger \mathbf{M}_2)$ is given by

$$Tr(\mathbf{M}_1^\dagger \mathbf{M}_2) = f^2 (g_{yy}g - g_y^2) f_{xx}g + g^2 (f_{xx}f - f_x^2) g_{yy}f, \quad (47)$$

and from (42) and (45) it is evident that $Tr(\mathbf{M}_1^\dagger \mathbf{M}_2) \geq 0$. Therefore, we can conclude that $\det(\nabla^2 h) \geq 0$. It remains to prove that $Tr(\nabla^2 h) \geq 0$ and it can easily be shown, since all diagonal components of $\nabla^2 h$ are positive. Consequently, we can see $\nabla^2 h \geq 0$ which means that $h(x, y)$ is a convex function and Lemma 1 is proved.

C. Proof of Proposition 1

First we show that $\hat{c}(x, y, d) = \log(\gamma)$ is convex, where

$$\begin{aligned} \gamma &= \left[\left(\frac{1}{1+x} \right) \left(\frac{1}{y} \right) + k \right] \frac{1}{d^\alpha}, \\ \gamma &= [f(x)g(y) + k] h(d) = q(x, y) h(d), \end{aligned}$$

where $f(x), g(y) > 0$. It can easily be proved that $\log\left(\frac{1}{1+x}\right), \log\left(\frac{1}{y}\right)$ are strictly convex. Then we have $\log(f(x)g(y))$ is strictly convex since it is a sum of two strictly convex functions. According to Lemma 1, it can be shown that $\log(q(x, y))$ is convex. Finally, $\log(\gamma) = \log(q(x, y)) + \log(h(d))$ is strictly convex due to it comprises the sum of strict convex functions. From the convexity of $\hat{c}(x, y, d)$, we can write

$$\nabla^2 \hat{c} = \begin{bmatrix} \frac{(q_{xx}q - q_x^2)}{q^2} & \frac{(q_{xy}q - q_x q_y)}{q^2} & 0 \\ \frac{(q_{yx}q - q_x q_y)}{q^2} & \frac{(q_{yy}q - q_y^2)}{q^2} & 0 \\ 0 & 0 & \frac{(h_{dd}h - h_d^2)}{h^2} \end{bmatrix}, \quad (48)$$

where $\nabla^2 \hat{c}$ is the Hessian matrix of \hat{c} , and q, h denotes the $q(x, y)$ and $h(d)$, respectively. q_x, q_{xy} stand for the partial derivative of q and are defined as $q_x = \frac{\partial q}{\partial x}$, $q_{xy} = \frac{\partial^2 q}{\partial x \partial y}$. $q_{xx}, q_{yy}, h_d, h_{dd}$ also are defined similarly. Due to $\nabla^2 \hat{c}$ is a PD (Positive Definite) matrix, so we have

$$\begin{aligned} q_{xx}q - q_x^2 > 0 &\Rightarrow q_{xx} > \frac{q_x^2}{q} > 0 \\ &\Rightarrow h \cdot q_{xx} > 0. \end{aligned} \quad (49)$$

Moreover, since $\log(f(x)g(y))$ is strictly convex, we can write

$$f_{xx}f > f_x^2, \quad g_{yy}g > g_y^2. \quad (50)$$

Then, we compute the Hessian matrix of $c(x, y, d) = \log(1 + \gamma)$ which takes the following form

$$\nabla^2 c = \frac{1}{(1 + q \cdot h)^2} (\mathbf{A} + \mathbf{B}),$$

where

$$\mathbf{A} = (q \cdot h)^2 \nabla^2 \hat{c},$$

$$\mathbf{B} = \begin{bmatrix} q_{xx}h & q_{xy}h & q_x h_d \\ q_{yx}h & q_{yy}h & q_y h_d \\ q_x h_d & q_y h_d & q h_{dd} \end{bmatrix}.$$

Matrix \mathbf{A} is PD since $\nabla^2 \hat{c}$ is PD and $q, h > 0$. In order to show that the Hessian matrix $\nabla^2 c$ is PD, we need to prove that \mathbf{B} is PD due to the sum of two PD matrices is PD. According to [31], if all upper left $n \times n$ determinants of a symmetric matrix are positive, the matrix is positive definite. Matrix \mathbf{B} is symmetric, since $q_{xy} = q_{yx} = f_x(x) g_y(y)$. Note, henceforth we drop the input variables of the functions for ease of exhibition (e.g. f stands for $f(x)$).

We start from the upper left 1×1 determinants of \mathbf{B} which equals to $q_{xx}h$. It follows from (49), that $q_{xx}h > 0$. Now, we proceed to show that the determinant of upper left 2×2 matrix of \mathbf{B} is positive. So, we can write

$$\frac{\det(\mathbf{B}_{2 \times 2})}{h^2} = (q_{xx} q_{yy} - q_{xy}^2) \quad (51)$$

$$\stackrel{(a)}{=} (f_{xx}f)(g_{xx}g) - f_x^2 g_y^2 \stackrel{(b)}{>} 0,$$

where $\mathbf{B}_{2 \times 2}$ denotes the upper left 2×2 matrix of \mathbf{B} . Step (a) holds by substituting $q_{xx} = f_{xx}g$, $q_{yy} = g_{yy}f$, $q_{xy} = f_x g_y$ in (51) and step (b) follows from (50). Then, we continue to compute the determinant of \mathbf{B} .

$$\det(\mathbf{B}) = h_d^2 \cdot (h \cdot m) + h_{dd}h \cdot (h \cdot q \cdot p),$$

where $m = 2q_{xy}q_x q_y - q_{xx}q_y^2 - q_{yy}q_x^2$, $p = q_{xx}q_{yy} - q_{xy}^2$. From (50), it can be shown that $m < 0$ and due to $\nabla^2 \hat{c}$ is a PD, we obtain

$$(q_{xx}q - q_x^2)(q_{yy}q - q_y^2) - (q_{xy}q - q_x q_y)^2 > 0$$

$$\Rightarrow m + q \cdot p > 0$$

$$\Rightarrow h \cdot m + h \cdot q \cdot p > 0$$

$$\Rightarrow h \cdot q \cdot p > -h \cdot m \quad (52)$$

Also, since $\log(h)$ is strictly convex, we can write

$$h_{dd}h > h_d^2. \quad (53)$$

Therefore, according to (52), (53) and the fact that $m < 0$, it can be seen that $\det(\mathbf{B}) > 0$. Since all upper left $n \times n$ determinants of \mathbf{B} are positive, we conclude that the matrix \mathbf{B} is PD. Finally, we can deduce that the $\nabla^2 c$ is PD which denotes the function $c(x, y, d)$ is convex.

REFERENCES

- [1] Y. Zeng, R. Zhang, and T. J. Lim, "Wireless communications with unmanned aerial vehicles: opportunities and challenges," *IEEE Communications Magazine*, vol. 54, no. 5, pp. 36–42, 2016.
- [2] M. Mozaffari, W. Saad, M. Bennis, and M. Debbah, "Unmanned aerial vehicle with underlaid device-to-device communications: Performance and tradeoffs," *IEEE Transactions on Wireless Communications*, vol. 6, no. 6, pp. 3949–3963, 2016.
- [3] E. Kalantari and H. Y. A. Yongacoglu, "On the number and 3D placement of drone base stations in wireless cellular networks," in *Vehicular Technology Conference (VTC-Fall), 2016 IEEE 84th*. IEEE, 2016, pp. 1–6.
- [4] E. Christy, R. P. Astuti, B. Syihabuddin, B. Narottama, O. Rhesa, and F. Rachmawati, "Optimum UAV flying path for Device-to-Device communications in disaster area," in *Signals and Systems (ICSigSys), 2017 International Conference on*. IEEE, 2017, pp. 318–322.
- [5] S. Hayat, E. Yanmaz, and R. Muzaffar, "Survey on unmanned aerial vehicle networks for civil applications: A communications viewpoint," *IEEE Communications Surveys & Tutorials*, vol. 18, no. 4, pp. 2624–2661, 2016.
- [6] B. V. der Bergh, A. Chiumento, and S. Pollin, "LTE in the sky: trading off propagation benefits with interference costs for aerial nodes," *IEEE Communications Magazine*, vol. 54, no. 5, pp. 44–50, 2016.
- [7] J. Chen and D. Gesbert, "Optimal positioning of flying relays for wireless networks: A LOS map approach," in *Communications (ICC), 2017 IEEE International Conference on*. IEEE, 2017, pp. 1–6.
- [8] O. Esrafilian and D. Gesbert, "Simultaneous User Association and Placement in Multi-UAV Enabled Wireless Networks," in *International ITG Workshop on Smart Antennas (WSA)*. IEEE, 2018.
- [9] L. Pawel, H. Oh, and W.-H. Chen, "Optimal positioning of communication relay unmanned aerial vehicles in urban environments," in *Unmanned Aircraft Systems (ICUAS), 2016 International Conference on*, 2016, pp. 1140–1147.
- [10] J. Park, H. Lee, S. Eom, and I. Lee, "Minimum Throughput Maximization in UAV-Aided Wireless Powered Communication Networks," *arXiv preprint arXiv:1801.02781*, 2018.
- [11] Wu, Qingqing, Y. Zeng, and R. Zhang, "Joint trajectory and communication design for multi-UAV enabled wireless networks," *IEEE Transactions on Wireless Communications*, vol. 17, no. 3, pp. 2109–2121, 2018.
- [12] A. Al-Hourani, S. Kandeepan, and S. Lardner, "Optimal LAP altitude for maximum coverage," *IEEE Wireless Communications Letters*, vol. 3, no. 6, pp. 569–572, 2014.
- [13] M. Mozaffari, W. Saad, M. Bennis, and M. Debbah, "Optimal transport theory for power-efficient deployment of unmanned aerial vehicles," in *Communications (ICC), 2016 IEEE International Conference on*. IEEE, 2016, pp. 1–6.
- [14] —, "Unmanned aerial vehicle with underlaid device-to-device communications: Performance and tradeoffs," *IEEE Transactions on Wireless Communications*, vol. 15, no. 6, pp. 3949–3963, 2016.
- [15] A. Al-Hourani, S. Kandeepan, and A. Jamalipour, "Modeling air-to-ground path loss for low altitude platforms in urban environments," in *Global Communications Conference (GLOBECOM), 2014 IEEE*, 2014, pp. 2898–2904.
- [16] E. Ostlin, H.-J. Zepernick, and H. Suzuki, "Macrocell path-loss prediction using artificial neural networks," *IEEE Transactions on Vehicular Technology*, vol. 59, no. 6, pp. 2735–2747, 2010.
- [17] J. Chen, U. Yatnalli, and D. Gesbert, "Learning radio maps for UAV-aided wireless networks: A segmented regression approach," in *IEEE International Conference on Communications (ICC)*. IEEE, 2017, pp. 1–6.
- [18] J. Chen, O. Esrafilian, D. Gesbert, and U. Mitra, "Efficient algorithms for air-to-ground channel reconstruction in UAV-aided communications," in *IEEE Globecom Workshop on Wireless Networking and Control for Unmanned Autonomous Vehicles*. IEEE, 2017, pp. 1–6.
- [19] O. Esrafilian and D. Gesbert, "3D city map reconstruction from UAV-based radio measurements," in *IEEE Global Communication Conference*. IEEE, 2017, pp. 1–6.
- [20] S. Rogers and M. Girolami, *A first course in machine learning*. CRC Press, 2016.
- [21] 3GPP TR 38.901 version 14.0.0 Release 14: "Study on channel model for frequencies from 0.5 to 100 GHz", ETSI, Tech. Rep., 2017.
- [22] D. P. Bertsekas, *Dynamic programming and optimal control*, 4th ed. Athena Scientific, 2017, vol. 1.
- [23] Y. Xu and W. Yin, "A block coordinate descent method for regularized multiconvex optimization with applications to nonnegative tensor factorization and completion," *SIAM Journal on imaging sciences*, vol. 6, no. 3, pp. 1758–1789.
- [24] Q. T. Dinh and M. Diehl, "Local convergence of sequential convex programming for nonconvex optimization," *Recent Advances in Optimization and its Applications in Engineering*, pp. 93–102, 2010.
- [25] A. Argyriou, "Link scheduling for multiple multicast sessions in distributed wireless networks," *IEEE Wireless Communications Letters*, vol. 2, no. 3, pp. 343–346, 2013.
- [26] H. Ju and R. Zhang, "Throughput maximization in wireless powered communication networks," *IEEE Transactions on Wireless Communications*, vol. 13, no. 1, pp. 418–428, 2014.

- [27] Z. Hadzi-Velkov, I. Nikoloska, G. K. Karagiannidis, and T. Q. Duong, "Wireless networks with energy harvesting and power transfer: Joint power and time allocation," *IEEE Signal Processing Letters*, vol. 23, no. 1, pp. 50–54, 2016.
- [28] M. Grant, S. Boyd, and Y. Ye, "CVX: Matlab software for disciplined convex programming, version 2.0 beta. <http://cvxr.com/cvx>." 2013.
- [29] E. D. Klerk, *Appendix A of Aspects of semidefinite programming: interior point algorithms and selected applications*. Springer Science & Business Media, 2006, vol. 65.
- [30] U. Prells, M. I. Friswell, and S. D. Garvey, "Use of geometric algebra: compound matrices and the determinant of the sum of two matrices." in *Proceedings of the Royal Society of London A: Mathematical, Physical and Engineering Sciences*, vol. 459, no. 2030. The Royal Society, 2003, pp. 273–285.
- [31] G. Strang, *Section 6.5 of Introduction to linear algebra*. Wellesley, MA: Wellesley-Cambridge Press, 1993, vol. 3.